remote sensing

MDPI

Technical Note

Fast Observation Operator for Global Navigation Satellite System Tropospheric Gradients

Florian Zus [1,*], Rohith Thundathil [1,2], Galina Dick [1] and Jens Wickert [1,2]

[1] GFZ German Research Centre for Geosciences, 14473 Potsdam, Germany; rohith@gfz-potsdam.de (R.T.); dick@gfz-potsdam.de (G.D.); wickert@tu-berlin.de (J.W.)
[2] Institute of Geodesy and Geoinformation Science, Technische Universität Berlin, 10623 Berlin, Germany
* Correspondence: zusflo@gfz-potsdam.de

Abstract: From the raw measurements at a single Global Navigation Satellite System (GNSS) ground-based station, the Zenith Total Delay (ZTD) and the tropospheric gradient can be estimated. In order to assimilate such data into Numerical Weather Prediction (NWP) models, the observation operator must be developed. Our previously developed tropospheric gradient operator is based on a linear combination of tropospheric delays and, therefore, is difficult to implement into NWP Data Assimilation (DA) systems. In this technical note, we develop a fast observation operator. This observation operator is based on an integral expression which contains the north–south and east–west horizontal gradients of refractivity. We run a numerical weather model (the horizontal resolution is 10 km) and show that for stations located in central Europe and in the warm season, the root-mean-square deviation between the tropospheric gradients calculated by the fast and original approach is about 0.15 mm. This deviation is regarded acceptable for assimilation since the typical root-mean-square deviation between observed and forward modelled tropospheric gradients is about 0.5 mm. We then implement the developed operator in our experimental DA system and test the proposed approach. In particular, we analyze the impact of the assimilation on the refractivity field. The developed tropospheric gradient operator, together with its tangent linear and adjoint version, is freely available (Fortran code) and ready to be implemented into NWP DA systems.

Keywords: GNSS; atmospheric remote sensing; zenith total delay; tropospheric gradient; observation operator; numerical weather prediction; data assimilation

Citation: Zus, F.; Thundathil, R.; Dick, G.; Wickert, J. Fast Observation Operator for Global Navigation Satellite System Tropospheric Gradients. *Remote Sens.* **2023**, *15*, 5114. https://doi.org/10.3390/rs15215114

Academic Editor: Michael E. Gorbunov

Received: 19 September 2023
Revised: 19 October 2023
Accepted: 25 October 2023
Published: 26 October 2023

1. Introduction

From the carrier phase and code measurements at a single Global Navigation Satellite System (GNSS) ground-based station, the Zenith Total Delay (ZTD) and the tropospheric gradient can be retrieved [1,2]. The ZTDs are available from station networks in (near) real time and numerous studies indicate that the assimilation of ZTDs improve short range weather forecasts. Therefore, several weather agencies assimilate ZTDs [3–5]. The ZTD contains information on the Integrated Water Vapor (IWV) above the station. This is the reason why ZTDs are beneficial, in particular, for rainfall monitoring and forecasting [6,7]. On the other hand, the ZTD at some station does not contain information about local gradients in the highly variable water vapor field. Tropospheric gradients do potentially provide additional information. However, they are currently not assimilated at weather agencies. The majority of published works deal with the (inter-technique) comparison of tropospheric gradients.

Ref. [2] presented preliminary results showing that the tropospheric gradients contain atmospheric features and do not solely absorb multipath, satellite orbit and clock errors in the analysis. However, the main focus was the positioning domain; a spurious improvement for the station repeatability was achieved when tropospheric gradients were taken into account in the analysis. Afterwards, researchers started to investigate the potential

of tropospheric gradients in meteorology. For a couple of stations, ref. [8] compared tropospheric gradients from GNSSs with tropospheric gradients derived from a Numerical Weather Model (NWM). The correlation between the GNSS and NWM tropospheric gradients was good for inland stations but not for stations close to the coast. Ref. [9] showed that the variation in tropospheric gradients follows the variation in the moisture field. This was investigated by the passage of a weather front. It was shown that the tropospheric gradients when plotted as vectors point from dry to moist areas. This was also shown by [10] studying deep convection. Ref. [11] used different software packages and compared the differences in the estimated tropospheric gradients for several stations on an island in the Mediterranean Sea. Recently, the quality of tropospheric gradients with high temporal resolution has been assessed by comparison to independent measurements such as a microwave radiometer [12]. To this end, the studies were limited to a handful of stations. Ref. [13] compared tropospheric gradients for hundreds of stations utilizing weather model data. The visual inspection of tropospheric gradient maps clearly showed that the GNSS's tropospheric gradients contain real atmospheric features. Ref. [13] studied the sensitivity of tropospheric gradients to several options in the processing. It turns out that the (near) real time estimation of tropospheric gradients is still challenging due to inaccurate satellite orbit and clocks. However, in post-processing mode, robust estimation of tropospheric gradients is possible.

Figure 1 shows a typical example for the GNSS and NWM tropospheric gradient map when large tropospheric gradients are present. Large tropospheric gradients often show up during severe weather events, and to make this visible the tropospheric gradient maps are overlaid with the radar data available from the Deutscher Wetter Dienst (DWD). In addition, the map showing the IWV values at the stations shows that the tropospheric gradients can be related to horizontal IWV gradients. It can be seen that tropospheric gradients point from dry to moist areas. In this particular example, the tropospheric gradients point into a strip of increased IWV extending across Germany. This convergence in the moister field is at least to some extent the reason for strong precipitation in accordance with the radar data.

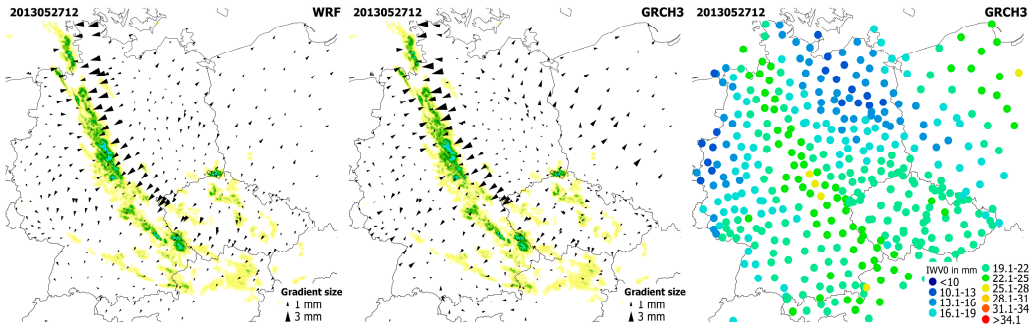

Figure 1. On 27 May 2013, 12 UTC large tropospheric gradients were present in central Europe. The **left** (**middle**) panel shows the NWM (GNSS) tropospheric gradient map. The tropospheric gradient maps are combined with radar precipitation data provided by the Deutscher Wetter Dienst (DWD). The radar precipitation data correspond to the instantaneous rain and is measured in mm/h. The color scale is yellow-green-blue-purple-red. The darker tone of a specific color means a higher rainfall intensity. The GNSS Integrated Water Vapor (IWV) map is shown in the **right** panel. Courtesy of Michael Kačmařík.

Comparisons such as those shown in Figure 1 triggered recent studies. The goal was to make use of the information contained in the tropospheric gradients. For example, the observation that tropospheric gradients are related to horizontal IWV gradients was utilized in order to show that the IWV interpolation is improved by utilizing tropospheric gradients [14]. Improved IWV fields are valuable for severe weather monitoring. However, it is the three-dimensional moisture field that is required in Numerical Weather Prediction (NWP). Therefore, we made a first attempt to estimate the impact of tropospheric gradients

in variational data assimilation [15]. In the preliminary study, we put a lot of emphasis on a systematic approach. We started the investigations with simulated observations before we used real observations. In addition, we considered three scenarios. In the first scenario, we assimilated ZTDs only. In the second scenario, we assimilated tropospheric gradients only. Finally, in the third scenario, we considered the assimilation of ZTDs and tropospheric gradients. This allowed us to show that the assimilation of tropospheric gradients in addition to the ZTDs improves the atmospheric fields. Though the results from this preliminary study were promising, a number of questions remained. In particular, the developed observation operator for tropospheric gradients is based on a combination of tropospheric delays. Such an observation operator is difficult to be implemented into NWP Data Assimilation (DA) systems. It is the purpose of this contribution to introduce a more simple and faster observation operator. The developed operator, together with its tangent linear and adjoint operator, is made available to be implemented into NWP DA systems.

Finally, we want to note that there are other ways to make use of tropospheric gradients in NWP. For example, ref. [16] proposed to take the GNSS zenith delay and tropospheric gradient estimates, assemble slant path delays (without the so-called post-fit-residuals added), perform a tomographic reconstruction of the refractivity field and then assimilate the resulting refractivity field into an NWM. The method we describe in this technical note is different in that we propose the direct assimilation of the GNSS zenith delay and tropospheric gradient estimates into an NWM.

Hence, this paper is structured as follows. In Section 2, we describe in brief how ZTDs and tropospheric gradients are estimated with the GNSS. This is important to better understand the observation modelling, i.e., the way we compute ZTDs and tropospheric gradients in an NWM. We show how our original tropospheric gradient operator works before we introduce our new approach: the fast tropospheric gradient operator. In Section 3, we compare the original and the fast approach, we compare measured and forward modelled tropospheric gradients and we show impact utilizing our experimental DA system. We discuss the results in Section 4 and provide the conclusion of this work in Section 5.

2. Materials and Methods

2.1. GNSS Zenith Total Delays and Tropospheric Gradients

In the processing of GNSS raw data, the tropospheric delay is approximated utilizing Mapping Functions (MF), zenith delays and tropospheric gradient components. In essence, for some elevation angle e and azimuth angle a, the tropospheric delay T is written as

$$T(e,a) = m_h(e) \cdot ZHD + m_w(e) \cdot ZWD + m_g(e) \cdot [cos(a) \cdot N + sin(a) \cdot E] \quad (1)$$

Here, ZHD is the Zenith Hydrostatic Delay, ZWD denotes the Zenith Wet Delay, m_h stands for the hydrostatic MF, m_w stands for the wet MF, N denotes the north gradient component and E denotes the east gradient component. The gradient MF is given by

$$m_g(e) = \frac{1}{\sin(e)\tan(e) + c} \quad (2)$$

where c is a constant [17]. The ZTD is obtained through

$$ZTD = ZHD + ZWD \quad (3)$$

The hydrostatic MF, the wet MF and the ZHD are typically derived from a climatology or a weather model [18–20]. The model for the tropospheric delay is plugged into the observation equation for the carrier phase (code) measurements and the ZWD, the north gradient component N and the east gradient component E are estimated together with the station coordinate, clock and other parameters in a common least square adjustment. Typically, the low elevation angle carrier phase (code) measurements are down-weighted to mitigate multipath effects and the error of the hydrostatic and wet MF. The error of the

a priori *ZHD* is largely compensated by the estimated *ZWD* so that the resulting *ZTD* is obtained with high accuracy. For details, refer to [20].

2.2. Original ZTD and Tropospheric Gradient Operator

The original ZTD and tropospheric gradient operator is based on tropospheric delays. We thus first explain in brief how the tropospheric delays are computed. For some station satellite link, the tropospheric delay S is obtained through

$$S = \int n ds - g \tag{4}$$

Here, n stands for the index of refraction, s denotes the arclength of the ray path and g stands for the geometric distance. The index of refraction n is calculated from the refractivity Ψ through

$$n = 10^{-6}\Psi + 1 \tag{5}$$

The refractivity is a function of the pressure, temperature and humidity [21]. The ray path follows from Fermat's principle: the path taken by the radio signal between two points is the path that can be traversed in the least time. In essence, the variation of the optical path length must vanish

$$\delta \int n \, ds = 0 \tag{6}$$

We neglect out-of-plane bending. This means that we assume that the ray path remains in the plane, which is defined by the station, the satellite and the center of the osculating sphere. Then, from variational calculus, it follows that the ray path between the station and the satellite $[x, z(x)]$ is obtained by solving the following differential equation [22]

$$\frac{d^2z(x)}{dx^2} - \left[\frac{n_z\,(x,z)}{n(x,z)} - \frac{n_x\,(x,z)}{n(x,z)}\frac{dz(x)}{dx}\right]\cdot\left[1 + \left(\frac{dz(x)}{dx}\right)^2\right] = 0 \tag{7}$$

where the subscripts indicate partial derivatives. Given the position of the station and the satellite, the boundary value problem is solved by a finite difference scheme [22].

For some station locations, we calculate 120 tropospheric delays. The spacing in azimuth is chosen to be 30° and the elevation angles are chosen to be 3°, 5°, 7°, 10°, 15°, 20°, 30°, 50°, 70°, 90°. Then, the ZTD operator denoted H_{ZTD}, the north gradient component operator denoted H_N and the east gradient component operator denoted H_E read as [20].

$$\begin{aligned} H_{ZTD} &= S(90°, 0°) \\ H_N &= \frac{\sum_{i=1}^{k} m_g(e_i) sin(e_i)^2 cos(a_i) S(e_i, a_i)}{\sum_{i=1}^{k} m_g(e_i)^2 sin(e_i)^2 cos(a_i)^2} \\ H_E &= \frac{\sum_{i=1}^{k} m_g(e_i) sin(e_i)^2 sin(a_i) S(e_i, a_i)}{\sum_{i=1}^{k} m_g(e_i)^2 sin(e_i)^2 sin(a_i)^2} \end{aligned} \tag{8}$$

where the indices indicate the specific azimuth and elevation angle.

The formula for the north gradient component and east gradient component is the result of a weighted least square adjustment [20]. The idea behind this weighted least square adjustment is to mimic the way tropospheric gradients are estimated in the GNSS analysis. Simulation studies justify this approach [20]. Another viewpoint is the following: we define the tropospheric gradient components (and ZTDs) according to our equation above and question ourselves whether it is possible to estimate such quantities with raw data collected at a ground based GNSS station. According to our simulation studies, the answer is yes [20]. In variational data assimilation, the tangent linear and adjoint operators are required too. The tangent linear code enables the computation of the total derivative and the adjoint code enables the computation of the partial derivative of the respective quantity with respect to the underlying control variables. In our case, the underlying

control variables are the pressure, temperature and water vapor field. The tangent linear (adjoint) operators are derived from the forward operator by rigorous application of the chain rule of differential calculus in forward (reverse) mode [23]. The tropospheric gradient operator can be interpreted as a specific linear combination of tropospheric delays. The coefficients of the linear combination do not depend on the control variables. Thus, the difficulty in the derivation of the tangent linear (adjoint) code comes from the difficulty of deriving the tangent linear (adjoint) code for the tropospheric delay. However, this task was already performed in one of our previous works [24].

The operator for the tropospheric gradient is costly since the computation of a single tropospheric gradient vector requires the calculation of 120 tropospheric delays. Therefore, we started to develop what we call the refined tropospheric gradient operator. This was done by two nearby simplifications: (1) we reduce the precision of the tropospheric delays that are utilized in the calculation of the tropospheric gradients, i.e., the number of nodes in the finite difference scheme is reduced and (2) we compute 30 instead of 120 tropospheric delays; the elevation angles are chosen to be 3°, 7°, 15°, 30° and 70° and the spacing in azimuth is chosen to be 60°. A single tropospheric delay is calculated for the elevation angle 90°. Comparing tropospheric gradients calculated by the refined and original operator lead to the conclusion that we can safely replace the original operator by the refined operator. The refined operator is tuned for efficiency. However, it is still based on dozens of tropospheric delays and, therefore, it remains difficult to be implemented into NWM DA systems

2.3. Fast ZTD and Tropospheric Gradient Operator

The fast tropospheric gradient operator is utilizing the closed-form proposed by [25] which depends on the north–south and east–west horizontal gradients of refractivity. This is rendering the calculation of tropospheric delays unnecessary. In essence, for some station locations, the ZTD operator, the north gradient component operator and the east gradient component operator read as

$$\begin{aligned} H_{ZTD} &= 10^{-6} \int \Psi \cdot dz \\ H_N &= 10^{-6} \int z \cdot \Psi_y \cdot dz \\ H_E &= 10^{-6} \int z \cdot \Psi_x \cdot dz \end{aligned} \tag{9}$$

where x, y and z denote the cartesian coordinates in the stations local horizon system. The subscripts indicate partial derivatives. The ZTD is identical to the previously introduced tropospheric delay in the zenith direction. The ZTD, the north gradient component and east gradient component are obtained by numerical integration over height and we utilize Simpson's rule for that purpose [22]. The key is the computation of the horizontal refractivity gradients Ψ_y and Ψ_x. At first, we express the horizontal refractivity gradients in terms of the station longitude λ and latitude ϕ.

$$\begin{aligned} \Psi_y &= \frac{\Psi_\phi}{r} \\ \Psi_x &= \frac{\Psi_\lambda}{r \cdot \cos\phi} \end{aligned} \tag{10}$$

where r denotes the radial distance (distance to the center of the osculating sphere). We propose to calculate the horizontal refractivity gradients by a least square adjustment. In essence, the refractivity Ψ and the horizontal refractivity gradients Ψ_ϕ and Ψ_λ at some altitude h are related to the vertically adjusted refractivity at the adjacent grid points of the NWM (Taylor series expansion).

$$\begin{aligned} \Psi_1 &= \Psi + (\lambda_1 - \lambda) \cdot \Psi_\lambda + (\phi_1 - \phi) \cdot \Psi_\phi \\ \Psi_2 &= \Psi + (\lambda_2 - \lambda) \cdot \Psi_\lambda + (\phi_2 - \phi) \cdot \Psi_\phi \\ &\cdots \\ \Psi_m &= \Psi + (\lambda_m - \lambda) \cdot \Psi_\lambda + (\phi_m - \phi) \cdot \Psi_\phi \end{aligned} \tag{11}$$

The vertically adjusted refractivity Ψ_i is obtained through vertical interpolation

$$\Psi_i = \Psi_i^k + \frac{\Psi_i^{k+1} - \Psi_i^k}{h_i^{k+1} - h_i^k} \left(h - h_i^k\right) \tag{12}$$

where Ψ_i^k and h_i^k denote the refractivity and the height for the kth level of the vertical profile ($k = 1, \ldots, q$), respectively. At and above the NWM top, the vertically adjusted refractivity Ψ_i is approximated by

$$\Psi_i = \Psi_i^q \cdot \exp\left[-G\frac{\left(h - h_i^q\right)}{T_i^n}\right] \tag{13}$$

where Ψ_i^q, T_i^q and h_i^q denote the refractivity, temperature and height at the NWM top, respectively, and G stands for the hydrostatic constant. The equation above is derived under the assumption that above the NWM top, the water vapor is negligible, the temperature is constant and the pressure follows from the hydrostatic equation and by approximating the geopotential height by geometric height. Given the vertically adjusted refractivity Ψ_i on the left hand side of Equation (11), the horizontal refractivity gradients Ψ_ϕ and Ψ_λ and the refractivity Ψ are determined by

$$\begin{pmatrix} \Psi \\ \Psi_\phi \\ \Psi_\lambda \end{pmatrix} = \left(M^T M\right)^{-1} M^T \left(\Psi_1, \ldots, \Psi_m\right) \tag{14}$$

where the coefficients of design matrix M are the partial derivatives of the right hand side of Equation (11) with respect to the refractivity and horizontal refractivity gradients. Let us define the matrix Γ by

$$\Gamma = \left(M^T M\right)^{-1} M^T, \tag{15}$$

then the resulting horizontal refractivity gradients Ψ_ϕ and Ψ_λ can be written as

$$\begin{aligned} \Psi_\phi &= \sum_{i=1}^{m} \Gamma_{2i} \cdot \Psi_i \\ \Psi_\lambda &= \sum_{i=1}^{m} \Gamma_{3i} \cdot \Psi_i \end{aligned} \tag{16}$$

The least square adjustment includes grid points inside a radius of about 35 km. For an NWM with a horizontal resolution of, e.g., 10 km, we have 8×8 grid points that are involved in the computation of the horizontal refractivity gradients. At first glance, the choice of grid points involved in the least square fit appears arbitrary. However, this choice is motivated by the observation geometry, i.e., the inverse cone made up of station satellite links. In fact, we experimented with the number of the grid points that are included in the least square adjustment. In the end, it is the comparison of the resulting tropospheric gradient components with the rigorously derived tropospheric gradient components that justifies our approach (see below). The tangent linear (adjoint) operators are derived from the forward operator by application of the chain rule of differential calculus in forward (reverse) mode. The fast gradient operator is a linear, depending on the refractivity field. In addition, in the construction of the tangent linear (adjoint) code, we ignore the dependency of the refractivity above the model top on the temperature. Therefore, the tangent linear and adjoint code construction is a straightforward task. Hence, as far as one is considered with the refractivity field (and not the humidity, pressure and temperature field separately), the fast gradient operator represents a linear forward operator. For further details, the reader is referred to the forward, tangent linear and adjoint code written in Fortran 90 and freely available (see Data Availability Statement).

2.4. WRF Model Simulations

The Weather Research and Forecasting (WRF) model [26] (version 3.9.1.1) is utilized to simulate the state of the atmosphere. The model domain covers the central part of Europe. The initial and boundary conditions are obtained from the Global Forecast System (GFS) analysis of the National Centers for Environmental Prediction (NCEP). The mesoscale model is initialized every day at 0 UTC and every day 24 h free forecasts are computed. The following parameterizations were utilized: for the microphysics, the Thompson scheme [27] was utilized; for the deep convection, the Kain–Fritsch scheme [28] was chosen; for the planetary boundary layer, the Yonsei University scheme [29] was applied; for the radiation, the Rapid Radiative Transfer Model (RRTM) Short and Longwave scheme [30] was utilized; the Unified Noah Land Surface Model [31] was chosen for the land surface model; and for the surface layer the revised Mesoscale Model 5 (MM5) scheme [32] was selected. The water vapor, temperature, pressure and geopotential field was stored every hour with a horizontal resolution of 10 km.

2.5. Experimental Data Assimilation System

This experimental system allows us to study the impact of various GNSS observations on the refractivity field by variational assimilation [15]. It does not allow us to study the impact on the water vapor, temperature and pressure field separately. The system works with simulated and real observations. When we work with simulated observations, it is as follows: we choose the true refractivity field, compute (error-free) zenith delays and tropospheric gradients, add noise in order to create observations, assimilate these observations into the background refractivity field and, in the last step, we check by how much the obtained analysis refractivity field is closer to the true refractivity field compared to the background refractivity field. When we utilize real observations, the workflow is the same except that simulated observations are replaced by real observations. The GFS analysis available with a horizontal resolution of 0.25° is regarded as the true refractivity field. The GFS 24 h forecast valid at the same time is regarded as the background refractivity field. The background error covariance matrix is estimated by calculating the difference between the GFS 24 h and 48 h forecast valid at the same time. For further details on the experimental DA system, refer to [15].

3. Results

3.1. Comparison of Fast and Original Tropospheric Gradient Operator

For this comparison, we select 400 stations covering Germany. The atmospheric fields are derived from WRF simulations which we ran for the time period June and July 2021. For each station location and every hour, we compute the tropospheric gradient components utilizing the original and fast tropospheric gradient operator. We then compare the tropospheric gradients components and quantify systematic and random deviations between the two approaches.

At first, we take a look on a map of the tropospheric gradient components. Figure 2 shows such a map for the north and east gradient component for an epoch where large tropospheric gradients are present. The tropospheric gradient components were calculated utilizing the original gradient operator. In these maps, the magnitude of the gradient components exceed 3 mm at specific locations and this indicates that large gradients are present in the refractivity field in the vicinity of the respective locations. The gradients in the refractivity field are mainly caused by gradients in the humidity field. This is usually the case in the warm season so that, roughly spoken, tropospheric gradient vectors point from dry to moist areas. Looking into the map of ZWDs supports this hypothesis. Figure 3 shows the north and east gradient component for the same epoch but now the east and north gradient components were calculated utilizing the fast gradient operator. The comparison of Figures 2 and 3 reveals that the tropospheric gradient maps from both approaches show a very similar pattern. In fact, the two approaches appear almost indistinguishable from

one another. However, there are some locations on the map where deviations can be noted and those are apparent when we have large gradient values.

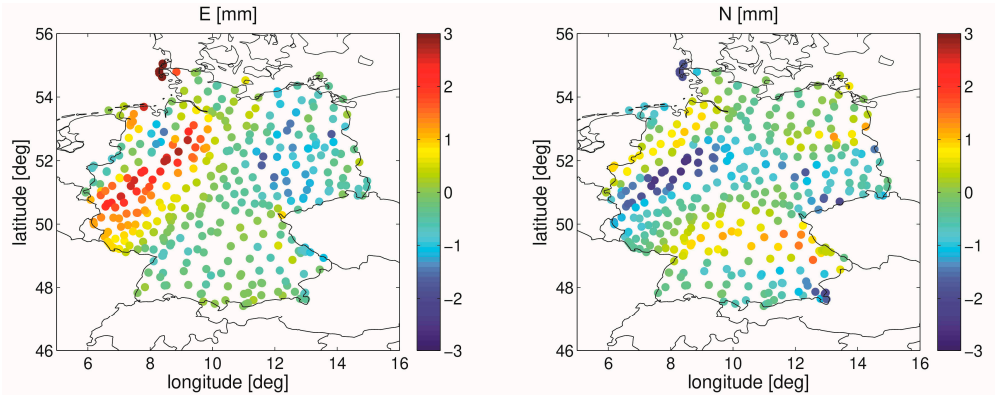

Figure 2. Map of tropospheric gradient components valid at 7.6.2021, 12 UTC. The original tropospheric gradient operator was utilized to derive the north and the east gradient component. The **left** (**right**) panel shows the **east** (**north**) gradient component.

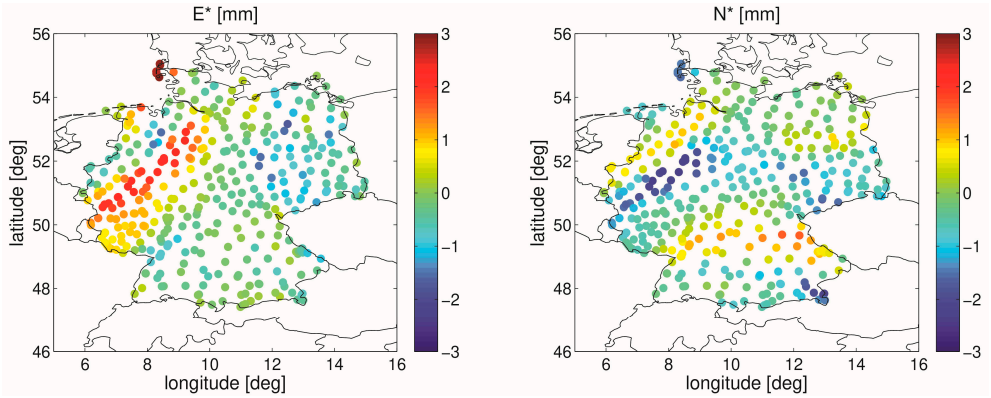

Figure 3. Same as Figure 2 but the fast tropospheric gradient operator was utilized to derive the north and the east gradient component.

Next we take a close look on the time series for a single station. The station is located in Potsdam, Germany. We show solely a zoom into the time series (June and July, 2021) so that details are visible. Figure 4 shows this zoom into the time series of the north and the east gradient components. The gradient components vary between 4 mm. Values close to zero indicate small variation in the local humidity field and large deviations from zero indicate large variations in the local humidity field. In such time series, the variations around zero appear random. However, tropospheric gradients maps, such as the one shown in Figure 1 (Figure 2 or Figure 3), clearly show that the peak values at specific locations and times are associated with specific atmospheric conditions such as the passage of warm and moist air masses (frontal systems) The different colors in the upper panel indicate the result for the two approaches: the fast and original approach. Again, it is difficult to distinguish the two approaches as the fast and the original approach yield similar east and north gradient components. When we form the difference between the tropospheric gradient components which is shown in the lower panel of Figure 4, we find that they can occasionally reach up to 0.9 mm.

Finally, we calculated the station specific mean and standard deviation between the two approaches for all stations. The station specific mean deviations are well below 0.1 mm for the tropospheric gradient components. The station specific standard deviations are typically about 0.15 mm for the tropospheric gradient components. Hence, we have random but no systematic deviations between the two approaches. By averaging over

all stations, we conclude that the observation error, i.e., the error of the fast observation operator, is about 0.15 mm. This is small compared with the typical standard deviation of about 0.5 mm we find between measured and forward modeled tropospheric gradient components (also see next section).

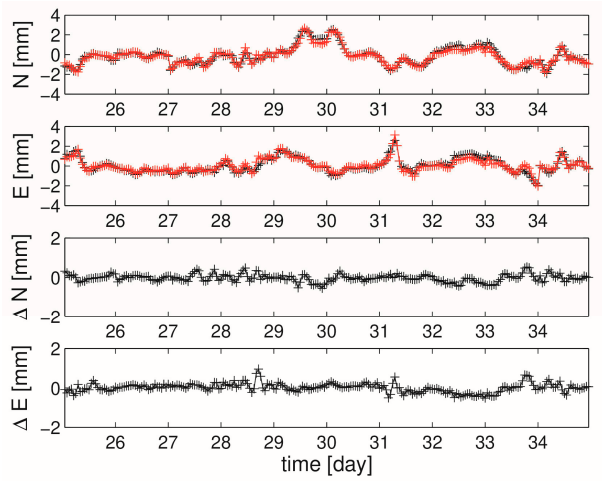

Figure 4. Zoom into the time series of the north and the east gradient components at the station POTS (Potsdam, Germany). The **upper** panel shows the tropospheric gradient components derived with the original (fast) observation operator in black (red) as a function of the time. The **lower** panel shows the differences between the tropospheric gradient components as a function of the time.

3.2. Comparison of NWM and GNSS Tropospheric Gradients

For this comparison, we select 250 stations which cover Germany, the Czech Republic and some parts of Austria and Poland (also see Figure 1). The GNSS data are taken from the Benchmark data set produced within the European COST Action ES1206 GNSS4SWEC (Advanced GNSS tropospheric products for monitoring severe weather and climate). For comprehensive information about the Benchmark data set, refer to [13]. We utilize the GNSS solution that is based on the G-Nut/Tefnut software [33] which is processing GNSS observations in Precise Point Positioning (PPP) [34] mode. For details on the GNSS processing, refer to [13]. The atmospheric fields are derived from WRF simulations which we ran for the time period May and June 2013. For each station location and every hour, we compute ZTDs and tropospheric gradient components. In the following, we call the computed (forward modeled) ZTDs and tropospheric gradients simply NWM ZTDs and tropospheric gradients. These NWM ZTDs and tropospheric gradients are then compared with the corresponding GNSS observation.

At first, we compare GNSS and NWM ZTDs. Figure 5 shows the station specific mean and standard deviation for the ZTD. The upper panel shows that for each station, the percentage number of measurements for the considered time period exceeds 75%. The mean deviations are mostly negative. On average, the mean deviation equals −3.7 mm. The standard deviations are around 11 mm. On average, the standard deviation equals 11.4 mm. Note that the ZTD for the considered area and season is about 2.5 m. Therefore, these numbers indicate good agreement between GNSS and NWM ZTDs and these numbers are consistent with the numbers provided by [13]. Hence, we expect good agreement for the east and the north gradient components as well.

Figure 6 shows the station specific mean and standard deviation for the north and the east gradient components, respectively. We note that the fast tropospheric gradient operator was applied. For both the east and the north gradient components, the mean deviations are close to zero. On average, the mean deviations are well below 0.1 mm. The standard deviations are around 0.5 mm. On average, the standard deviation for the east and the north gradient components equals 0.57 mm and 0.55 mm, respectively. Again, these numbers are consistent with the numbers provided by [13]. Figure 7 shows the station

specific mean and standard deviation for the north and the east gradient components, respectively. In this comparison, the original tropospheric gradient operator was applied. For both the east and the north gradient components, the mean deviations are close to zero. On average, the mean deviations are well below 0.1 mm. The standard deviations are around 0.5 mm. On average, the standard deviation for the east and the north gradient components equals 0.56 mm and 0.52 mm, respectively. Hence, the standard deviations when we applied the original tropospheric gradient operator are somewhat smaller than the standard deviations when we applied the fast observation operator. However, as far as we are concerned with the statistics, it does not matter whether we apply the original or the fast tropospheric gradient operator.

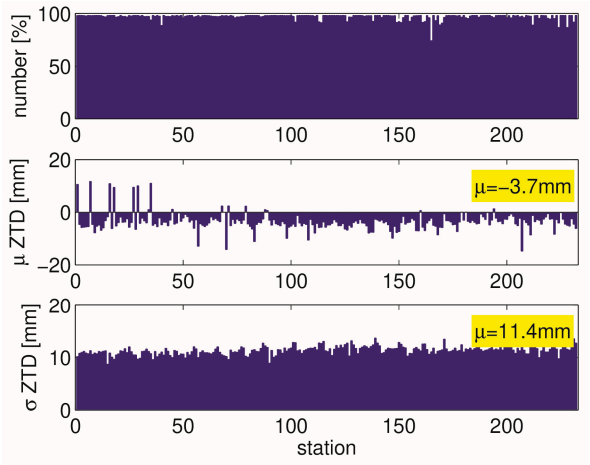

Figure 5. We compare GNSS and NWM ZTDs for a two month period (May and June 2013). The 250 stations cover Germany, the Czech Republic and parts of Austria and Poland. The **upper** panel shows the data availability in percent per station. The **middle** panel shows the station specific mean deviation. The **lower** panel shows the station specific standard deviation. The number (yellow background) equals the average value of the respective parameter.

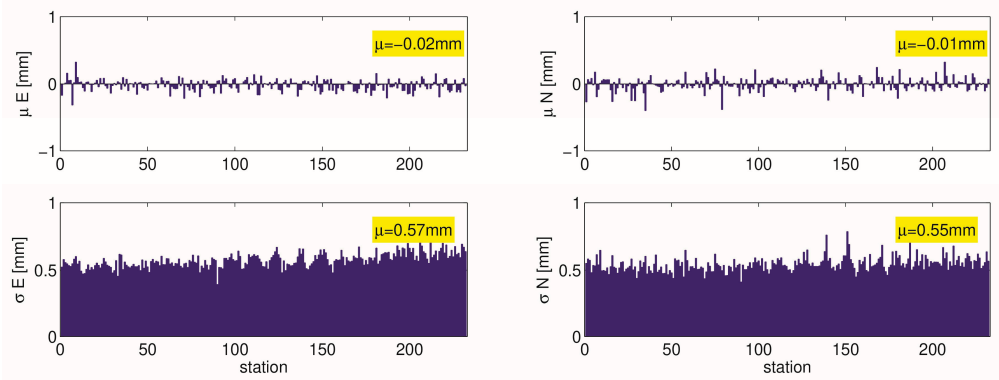

Figure 6. We compare GNSS and NWM tropospheric gradient components for a two month period (May and June 2013). The 250 stations cover central Europe. The fast tropospheric gradient operator is utilized for this comparison. The **left** (**right**) panel shows the statistic for the **east** (**north**) gradient components. The **upper** panel shows the station specific mean deviation. The **lower** panel shows the station specific standard deviation. The number (yellow background) equals the average value of the respective parameter.

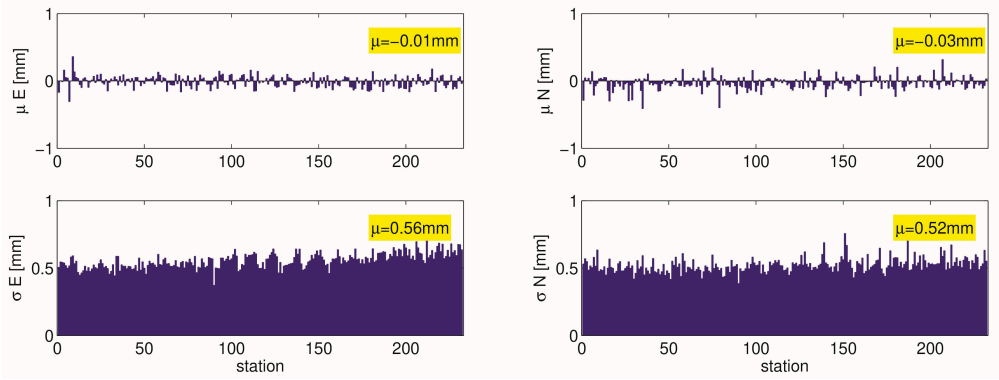

Figure 7. Same as Figure 6 but the original tropospheric gradient operator is utilized for this comparison.

3.3. Results from Our Experimental Data Assimilation System

We assimilate data four times per day (0, 6, 12, 18 UTC) for a period of four months (May, June, July, August, 2021). We consider simulated and real observations from the station Potsdam, Germany. The workflow of the assimilation experiment is as follows: (1) Compute true ZTDs and tropospheric gradients from the GFS analysis and write them to disk. The original operator is used. (2) Import the true ZTDs and tropospheric gradients and add noise, i.e., 10 mm for the ZTDs and 0.5 mm for the tropospheric gradients. (3) Assign observation errors; 10 mm for the ZTDs and 0.5 mm for the tropospheric gradients. (4) Assimilate the observed ZTDs and tropospheric gradients into the GFS 24 h forecast valid at the same time. Here, we distinguish two possibilities: the original operator or the fast operator can be utilized. We note that for both operators, the same observation error of 0.5 mm is applied as we do not find a significant difference in the observation minus background statistic (also see Section 3.2 above). (5) Check the refractivity error in the vicinity of the station. When we utilize real observation, we omit step two and utilize the GNSS solution that is provided by the Nevada Geodetic Laboratory (NGL) [35]. This GNSS solution is based on the GipsyX software [36] and is processing GNSS observations in PPP mode. For details on the GNSS processing, refer to [35].

The impact of the various types (and combinations) of GNSS observations in variational data assimilation is measured by analyzing the refractivity profiles surrounding the station [15]. We restrict our discussion to the case where we assimilate real observations. We obtain similar results for the case where we assimilate simulated observations. The experiment with simulated observations fully supports all main findings from the experiment with real observations. Figure 8 shows the root-mean-square error of the background refractivity (black line), the root-mean-square error of the refractivity when we assimilate ZTDs only (blue line) and the root-mean-square error of the refractivity when we assimilate both ZTDs and tropospheric gradients (red line) as a function of the pressure. The original tropospheric gradient operator is utilized in this experiment. It can be seen that there is an improvement when the ZTDs are assimilated and that there is a further improvement when the tropospheric gradients are assimilated together with the ZTDs. The impact of the tropospheric gradient assimilation is restricted to altitudes around 750 hPa. This is consistent with what we found in our previous work [15]. Next, instead of the original tropospheric gradient operator, the fast tropospheric gradient operator is utilized in the experiment. Figure 9 shows the root-mean-square error of the background refractivity (black line), the root-mean-square error of the refractivity when we assimilate ZTDs only (blue line) and the root-mean-square error of the refractivity when we assimilate both ZTDs and tropospheric gradients (red line) as a function of the pressure. Again, it can be seen that there is an improvement when the tropospheric gradients are assimilated in addition to the ZTDs and again, the impact of the tropospheric gradient assimilation is restricted to an altitude around 750 hPa. It appears that the impact is somewhat smaller below 750 hPa but somewhat larger above 750 hPa. We do not obtain exactly the same impact for both

tropospheric gradient operators, but as the impact is similar for both cases, we conclude that the fast gradient operator is applicable. The formula for the fast tropospheric gradient operator makes clear why we have small impact at low altitudes: the horizontal refractivity gradients are weighted by height above the station, and when the height above the station is close to zero, the contribution to the integral is close to zero. Therefore, unlike the ZTDs, tropospheric gradients are not sensitive to the near surface variables. This implies that the assimilation of tropospheric gradients does not affect surface variables. The main impact can be found somewhere around 800 hPa [15].

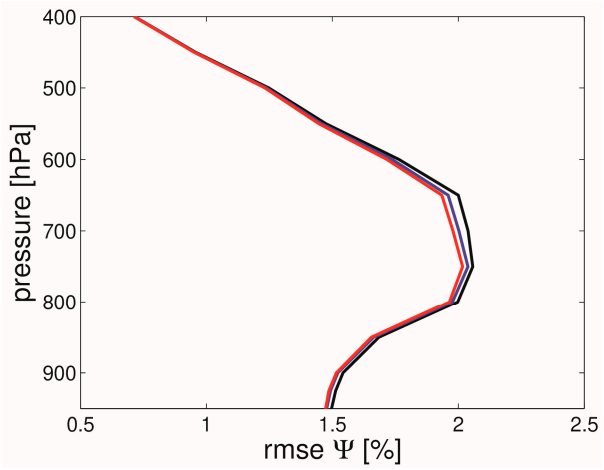

Figure 8. The root-mean-square error of the refractivity in percent as a function of the pressure. The black line corresponds to the background, the blue line corresponds to the case when ZTDs are assimilated and the red line corresponds to the case where both ZTDs and tropospheric gradients are assimilated. GNSS ZTDs and tropospheric gradients for the single station Potsdam are assimilated four times per day (0, 6, 12, 18 UTC) for a period of four months (May, June, July and August 2021). The original tropospheric gradient operator is utilized in the assimilation.

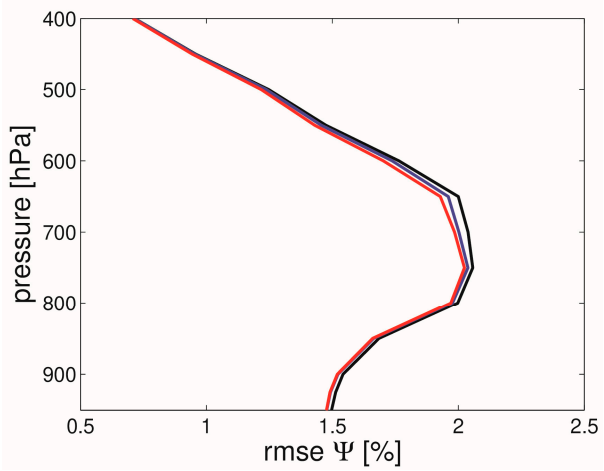

Figure 9. Same as Figure 8 but the fast tropospheric gradient operator is utilized in the assimilation.

4. Discussion

The ZTD and the tropospheric gradients can be measured with a single ground-based GNSS station. In order to make use of such observations in NWP, the forward operators must be implemented into DA systems. Notably, in variational data assimilation, besides the forward operator, the tangent linear and adjoint version of the operator are required too. Where this task is straightforward for the ZTD, it is not straightforward for the tropospheric gradient components. Our original tropospheric gradient operator [15] is complicated as it is based on dozens of ray-traced tropospheric delays. Therefore, in this work, we introduce

an alternative approach which we call the fast tropospheric gradient operator. This is rendering the calculation of ray-traced tropospheric delays unnecessary. We utilize the WRF model (horizontal resolution of 10 km) and compare the original and the fast approach. We find a random deviation of about 0.15 mm between the two approaches. The systematic deviation between the two approaches is negligible. We also compare forward modelled and measured tropospheric gradients and found negligible differences in the statistics for the two approaches. We then implemented the fast tropospheric gradient operator in our experimental DA system. With this experimental DA system, we cannot run actual weather forecasts. The main purpose of it is to give a glimpse on the impact of various types of observations on (initial) refractivity fields. Again, we demonstrated that the assimilation of tropospheric gradients on top of the assimilation of the ZTD improves the refractivity field in the vicinity of the station. In particular, we show that it does not matter which tropospheric gradient operator is utilized in the assimilation. In essence, when we utilize the fast tropospheric gradient operator, we find similar impact than when we utilize the original (rigorous) tropospheric gradient operator. Clearly, as the functional dependency of the fast tropospheric gradient operator from the refractivity is different than the functional dependency of the original tropospheric gradient operator from the refractivity, the impact is not the same. Our results are representative for stations in central Europe and in the warm season. Whether adaptation of the fast gradient operator is required for different regions and seasons must be analyzed in future work.

5. Conclusions

In this study, we developed an efficient tropospheric gradient operator (a piece of Fortran code). The advantage of the proposed tropospheric gradient operator over the original (rigorous) tropospheric gradient operator is that it does not require the calculation of dozens of ray-traced tropospheric delays. Together with the tangent linear and adjoint operator, it is ready to be implemented into DA systems. The source codes are freely available (see Data Availability Statement). The source codes are snippets from our experimental DA system so some adaptation is required when implemented into another DA system. However, the source codes certainly help to better understand the details and the ease of implementation of the proposed approach. In future, we will implement the operator into sophisticated DA systems. In fact, recently the operator was implemented into the WRF DA system in support of the project EGMAP ('Exploitation of GNSS tropospheric gradients for severe weather monitoring and prediction') funded by the German Research Foundation (DFG).

Author Contributions: Conceptualization, F.Z.; methodology, F.Z.; software, F.Z. and R.T.; validation, F.Z.; formal analysis, F.Z.; investigation, F.Z.; resources, F.Z. and R.T.; data curation, F.Z. and R.T.; writing—original draft preparation, F.Z.; writing—review and editing, F.Z., R.T., G.D. and J.W.; visualization, F.Z.; supervision, G.D. and J.W. All authors have read and agreed to the published version of the manuscript.

Funding: This research received no external funding.

Data Availability Statement: The source code for the fast tropospheric gradient operator together with the tangent linear and adjoint version (Fortran 90) is available via ftp://ftp.gfz-potsdam.de/pub/home/GNSS/products/gfz-tgra/ (accessed on 25 February 2023).

Acknowledgments: The Global Forecast System data are provided by the National Centres for Environmental Prediction (https://www.nco.ncep.noaa.gov/pmb/products/gfs/ (accessed on 25 February 2023)). The GNSS data are provided by the Geodetic Observatory Pecny (GOP) (http://www.pecny.cz (accessed on 25 February 2023)) and the Nevada Geodetic Laboratory (NGL) (http://geodesy.unr.edu/ (accessed on 25 February 2023)). We thank Michal Kačmařík for preparing the radar image plus tropospheric gradient map and for preparing the GNSS data set in a user friendly format.

Conflicts of Interest: The authors declare no conflict of interest.

References

1. Bevis, M.; Businger, S.; Herring, T.A.; Rocken, C.; Anthes, R. A.; Ware, R. GPS meteorology: Remote sensing of atmospheric water vapor using the Global Positioning System. *J. Geophys. Res.* **1992**, *97*, 15787–15801. [CrossRef]
2. Bar-Sever, Y.E.; Kroger, P.M.; Borjesson, J.A. Estimating horizontal gradients of tropospheric path delay with a single GPS receiver. *J. Geophys. Res.* **1998**, *103*, 5019–5035. [CrossRef]
3. Poli, P.; Moll, P.; Rabier, F.; Desroziers, G.; Chapnik, B.; Berre, L.; Healy, S.B.; Andersson, E.; El Guelai, F.-Z. Forecast impact studies of zenith total delay data from European near real-time GPS stations in Meteo France 4DVAR. *J. Geophys. Res.* **2007**, *112*, D06114. [CrossRef]
4. Bennitt, G.V.; Jupp, A. Operational assimilation of GPS zenith total delay observations into the Met Office Numerical Weather Prediction models. *Mon. Weather Rev.* **2012**, *140*, 2706–2719. [CrossRef]
5. Mahfouf, J.-F.; Ahmed, F.; Moll, P.; Teferle, F.N. Assimilation of zenith total delays in the AROME France convective scale model: A recent assessment. *Tellus A Dyn. Meteorol. Oceanogr.* **2015**, *67*, 26106. [CrossRef]
6. Zhao, Q.; Liu, K.; Sun, T.; Yao, Y.; Li, Z. A novel regional drought monitoring method using GNSS-derived ZTD and precipitation. *Remote Sens. Environ.* **2023**, *297*, 113778. [CrossRef]
7. Gong, Y.; Liu, Z.; Chan, P.W.; Hon, K.K. Assimilating GNSS PWV and radiosonde meteorological profiles to improve the PWV and rainfall forecasting performance from the Weather Research and Forecasting (WRF) model over the South China. *Atmos. Res.* **2023**, *286*, 106677. [CrossRef]
8. Walpersdorf, A.; Calais, E.; Haase, J.; Eymard, L.; Desbois, M.; Vedel, H. Atmospheric Gradients Estimated by GPS Compared to a High Resolution Numerical Weather Prediction (NWP) Model. *Phys. Chem. Earth* **2001**, *26*, 147–152. [CrossRef]
9. Iwabuchi, T.; Miyazaki, S.; Heki, K.; Naito, I.; Hatanaka, Y. An impact of estimating tropospheric delay gradients on tropospheric delay estimations in the summer using the Japanese nationwide GPS array. *J. Geophys. Res.* **2003**, *108*, 4315. [CrossRef]
10. Brenot, H.; Neméghaire, J.; Delobbe, L.; Clerbaux, N.; De Meutter, P.; Deckmyn, A.; Delcloo, A.; Frappez, L.; Van Roozendael, M. Preliminary signs of the initiation of deep convection by GNSS. *Atmos. Chem. Phys.* **2013**, *13*, 5425–5449. [CrossRef]
11. Morel, L.; Pottiaux, E.; Durand, F.; Fund, F.; Boniface, K.; de Oliveira, P.S.; Van Baelen, J. Validity and behaviour of tropospheric gradients estimated by GPS in Corsica. *Adv. Space Res.* **2015**, *55*, 135–149. [CrossRef]
12. Ning, T.; Elgered, G. High-temporal-resolution wet delay gradients estimated from multi-GNSS and microwave radiometer observations. *Atmos. Meas. Tech.* **2021**, *14*, 5593–5605. [CrossRef]
13. Kačmařík, M.; Douša, J.; Zus, F.; Václavovic, P.; Balidakis, K.; Dick, G.; Wickert, J. Sensitivity of GNSS tropospheric gradients to processing options. *Ann. Geophys.* **2019**, *37*, 429–446. [CrossRef]
14. Zus, F.; Douša, J.; Kačmařík, M.; Václavovic, P.; Balidakis, K.; Dick, G.; Wickert, J. Improving GNSS Zenith Wet Delay Interpolation by Utilizing Tropospheric Gradients: Experiments with a Dense Station Network in Central Europe in the Warm Season. *Remote Sens.* **2019**, *11*, 674. [CrossRef]
15. Zus, F.; Douša, J.; Kačmařík, M.; Václavovic, P.; Dick, G.; Wickert, J. Estimating the Impact of Global Navigation Satellite System Horizontal Delay Gradients in Variational Data Assimilation. *Remote Sens.* **2019**, *11*, 41. [CrossRef]
16. Hanna, N.; Trzcina, E.; Möller, G.; Rohm, W.; Weber, R. Assimilation of GNSS tomography products into the Weather Research and Forecasting model using radio occultation data assimilation operator. *Atmos. Meas. Tech.* **2019**, *12*, 4829–4848. [CrossRef]
17. Chen, G.; Herring, T.A. Effects of atmospheric azimuthal asymmetry on the analysis of space geodetic data. *J. Geophys. Res.* **1997**, *102*, 20489–20502. [CrossRef]
18. Boehm, J.; Heinkelmann, R.; Schuh, H. Short Note: A global model of pressure and temperature for geodetic applications. *J. Geod.* **2007**, *81*, 679–683. [CrossRef]
19. Boehm, J.; Niell, A.; Tregoning, P.; Schuh, H. Global mapping function (GMF): A new empirical mapping function based on numerical weather model data. *Geophys. Res. Lett.* **2006**, *33*, 943–951. [CrossRef]
20. Zus, F.; Balidakis, K.; Dick, G.; Wilgan, K.; Wickert, J. Impact of Tropospheric Mismodelling in GNSS Precise Point Positioning: A Simulation Study Utilizing Ray-Traced Tropospheric Delays from a High-Resolution NWM. *Remote Sens.* **2021**, *13*, 3944. [CrossRef]
21. Thayer, G.D. An improved equation for the radio refractive index of air. *Radio Sci.* **1974**, *9*, 803–807. [CrossRef]
22. Zus, F.; Dick, G.; Douša, J.; Heise, S.; Wickert, J. The rapid and precise computation of GPS slant total delays and mapping factors utilizing a numerical weather model. *Radio Sci.* **2014**, *49*, 207–216. [CrossRef]
23. Giering, R.; Kaminski, T. Recipes for adjoint code construction, ACM Trans. *Math. Softw.* **1998**, *24*, 437–474. [CrossRef]
24. Zus, F.; Dick, G.; Heise, S.; Wickert, J. A forward operator and its adjoint for GPS slant total delays. *Radio Sci.* **2015**, *50*, 393–405. [CrossRef]
25. Davis, J.; Elgered, G.; Niell, A.; Kuehn, K. Ground-based measurement of gradients in the "wet" radio refractivity of air. *Radio Sci.* **1993**, *28*, 1003–1018. [CrossRef]
26. Skamarock, W.C.; Klemp, J.B.; Dudhia, J.; Gill, D.O.; Barker, D.M.; Duda, M.G.; Huang, X.Y.; Wang, W.; Powers, J.G. *A Description of the Advanced Research WRF Version 3*; NCAR tech. note NCAR/TN-475+STR; NCAR: Boulder, CO, USA, 2008. [CrossRef]
27. Thompson, G.; Field, P.R.; Rasmussen, R.M.; Hall, W.D. Explicit Forecasts of Winter Precipitation Using an Improved Bulk Microphysics Scheme. Part II: Implementation of a New Snow Parameterization. *Mon. Weather Rev.* **2008**, *136*, 5095–5115. [CrossRef]
28. Kain, J.S. The Kain–Fritsch convective parameterization: An update. *J. Appl. Meteorol.* **2004**, *43*, 170–181. [CrossRef]

29. Hong, S.Y.; Noh, Y.; Dudhia, J. A new vertical diffusion package with an explicit treatment of entrainment processes. *Mon. Weather Rev.* **2006**, *134*, 2318–2341. [CrossRef]
30. Iacono, M.J.; Delamere, J.S.; Mlawer, E.J.; Shephard, M.W.; Clough, S.A.; Collins, W.D. Radiative forcing by long–lived greenhouse gases: Calculations with the AER radiative transfer models. *J. Geophys. Res.* **2008**, *113*, D13103. [CrossRef]
31. Tewri, M.; Chen, F.; Wang, W.; Dudhia, J.; LeMone, M.A.; Mitchell, K.; Ek, M.; Gayno, G.; Wegiel, J.; Cuenca, R.H. Implementation and verification of the unified NOAH land surface model in the WRF model. In Proceedings of the 20th Conference on Weather Analysis and Forecasting/16th Conference on Numerical Weather Prediction, Seattle, WA, USA, 12–16 January 2004; pp. 11–15.
32. Jimenez, P.A.; Jimy Dudhia, J.; Gonzalez-Rouco, F.; Navarro, J.; Montavez, J.P.; Garcia-Bustamante, E. A revised scheme for the WRF surface layer formulation. *Mon. Weather Rev.* **2012**, *140*, 898–918. [CrossRef]
33. Václavovic, P.; Douša, J. Backward smoothing for precise GNSS applications. *Adv. Space Res.* **2015**, *56*, 1627–1634. [CrossRef]
34. Zumberge, J.F.; Heflin, M.B.; Jefferson, D.C.; Watkins, M.M.; Webb, F.H. Precise point positioning for the efficient and robust analysis of GPS data from large networks. *J. Geophys. Res.* **1997**, *102*, 5005–5017. [CrossRef]
35. Blewitt, G.; Hammond, W.C.; Kreemer, C. Harnessing the GPS data explosion for interdisciplinary science. *Eos* **2018**, *99*. [CrossRef]
36. Bertiger, W.; Bar-Sever, Y.; Dorsey, A.; Haines, B.; Harvey, N.; Hemberger, D.; Heflin, M.; Lu, W.; Miller, M.; Moore, A.W.; et al. GipsyX/RTGx, a new tool set for space geodetic operations and research. *Adv. Space Res.* **2020**, *66*, 469–489. [CrossRef]